FISEVIER

Contents lists available at ScienceDirect

Carbon

journal homepage: www.elsevier.com/locate/carbon



Friction at single-layer graphene step edges due to chemical and topographic interactions



Lei Chen ^{a, 1}, Zhe Chen ^{b, 1}, Xiaoyu Tang ^a, Wenmeng Yan ^a, Zhongrong Zhou ^a, Linmao Qian ^{a, *}, Seong H. Kim ^{a, b, **}

- ^a Tribology Research Institute, State Key Laboratory of Traction Power, Southwest Jiaotong University, Chengdu, 610031, China
- b Department of Chemical Engineering and Materials Research Institute, Pennsylvania State University, University, Park, PA, 16802, USA

ARTICLE INFO

Article history: Received 10 June 2019 Received in revised form 18 July 2019 Accepted 23 July 2019 Available online 24 July 2019

ABSTRACT

Although graphene is well known for super-lubricity of its basal plane, friction at its step edge is not well understood. In this study, friction of a single-layer graphene step edge was studied using atomic force microscopy (AFM) in vacuum and humid air conditions. At a 0.34 nm thick graphene step edge, friction varies drastically depending on whether it is exposed at the topmost surface or covered under other graphene layers. The friction response of the step edge buried under one layer of graphene can be fully explained with the topographic effect only; in contrast, the exposed step edge exhibits both topographic and chemical contributions to friction. Chemical characterizations suggest that the exposed graphene step edge is terminated with C—OH groups, which can interact with the AFM tip surface through hydrogen bonding interactions and thus increase friction. The chemical interactions at the exposed step edge significantly amplify the topographic effect. When the step edge is covered by more than one layer of graphene, friction is not sensitive to the 0.34 nm height change. This must be due to the stiffness of multilayer graphene and the height changes gradually at the step edge. These findings will advance fundamental knowledge of the frictional behaviors of graphene.

© 2019 Elsevier Ltd. All rights reserved.

1. Introduction

Graphene is well known for superior strength, which makes it an ideal material for ultra-thin protective coatings from nanoscale to macroscale [1–6]. Due to the ultra-low topographic corrugation of the graphene (and graphite) basal plane as well as incommensurate contact with other materials, extremely low coefficient of friction (COF) or super-lubricity can be achieved [7–9]. Because the single layer graphene is only 0.34 nm thick, friction response on the graphene basal plane can be altered by the low bending modulus as the graphene thickness decreases to a few layers [10]; friction can also be affected by the substrate roughness [11] and the intercalation of molecules between the graphene layer and the substrate

[12,13]. Moreover, the friction properties of graphene depend on the environmental conditions [14] and chemical modification [15,16]. In practical applications of graphene as solid lubricant coatings, another complexity is encountered. Unless the entire substrate surface is covered conformally with only one piece of defect-free graphene, corrugated features can always be found at graphene-covered surfaces. Such corrugated features include folds, wrinkles, blisters, step edges, and so on. Among these features, graphene step edges can cause extremely high friction compared to the basal plane and significantly deteriorate the overall lubricity of the graphene coating [17–30]. Thus, it is important to understand the origin of the high friction at the graphene step edge.

Since the step edge of a single graphene layer is so sharp laterally (widthwise, less than one covalent bond length) and only 0.34 nm tall vertically, only nanoscale measurements with atomic force microscope (AFM) can properly assess the friction behavior at single layer graphene step edges [31–33]. Previous studies agreed that when the AFM tip moves up from the lower terrace of the step edge to the upper terrace, friction is significantly larger than that on the basal plane [17–30]. However, in the case of the tip sliding down the step edge from the upper terrace to the lower terrace, two

^{*} Corresponding author. Tribology Research Institute, State Key Laboratory of Traction Power, Southwest Jiaotong University, Chengdu 610031, China.

^{**} Corresponding author. Department of Chemical Engineering and Materials Research Institute, Pennsylvania State University, University Park, PA, 16802, USA.

E-mail addresses: linmao@swjtu.edu.cn (L. Qian), shkim@engr.psu.edu (S.H. Kim).

¹ These authors contributed equally to this work.

opposite trends have been reported. While most papers reported an increase in friction during the step-down [17–27], a few papers reported a negative friction which means the tip is pushed forward along the sliding direction [28,29]. The latter case could be explained with the topographic effect; in other words, the forwarddirection force is produced due to the height difference (geometry). In order to explain the former case (resistive force during the stepdown process), a concept of a high potential barrier at the step edge, which is often called Ehrlich-Schwoebel barrier [34], was introduced [21,24,28]. Although this model could reproduce the general trend of the resistive force for the step-down process, the origin of the large additional barrier is not well documented or explained. Others attempted to explain this resistive force by arguing the presence of dangling bonds at the graphene step edge, because they are expected to have strong chemical interactions with the tip surface [18,30]. Without proper characterization of functional groups at the graphene step edge, the presence of undercoordinated carbon atoms was often assumed in complementary molecular dynamics simulations [19,28,29,35]. In some reports, friction measurements were performed with a scan size of hundreds of nanometers [18,22,24,25,27,28,30] or a poor signal-tonoise ratio [19,29]; thus, detailed information could have been missed due to the low resolution of analysis. This led to some discrepancy in experimental data and incomplete understanding of frictional behaviors originating from chemical interactions between the graphene step edge and the counter surface.

In this study, we report clear distinction between the purely topographic effect and the convoluted effect of chemical and topographic contributions. This distinction was possible by identifying the functional groups at the graphene step edge exposed to air and comparing frictions at the exposed step edges and the step edges buried under graphene layers. The freshly-cleaved graphite surface exposing graphene basal planes and step edges was characterized with x-ray photoelectron spectroscopy (XPS) and polarization-modulation reflection-absorption infrared spectroscopy (PM-RAIRS). Then, nanoscale friction behaviors of the graphene step edge were measured using AFM with a clean and sharp Si₃N₄ tip (Fig. S1). The data presented here provide an insight into fundamental processes governing friction at the graphene step edge, proving that the friction is influenced by both chemical and topographic effects and these two effects can be well differentiated. These findings enrich the understanding of the friction behavior of graphene surfaces.

2. Experimental

2.1. Graphite surface preparation and characterization

A freshly-cleaved graphite surface was produced on a highlyoriented pyrolytic graphite (HOPG) crystal by tape-exfoliation in ambient air. Immediately after exfoliation, the sample was transferred into the vacuum chamber of the XPS system. The XPS analysis was performed using a PHI VersaProbe system equipped with a monochromatic Al-Ka x-ray source. The HOPG crystal was mounted on the sample stage with a metal clip and no sputter cleaning was performed on the graphite surface. The freshly-cleaved graphite surface was also analyzed with PM-RAIRS in a humidity controlled chamber. PM-RAIRS measurements were carried out using a Thermo-Nicolet Nexus 670 spectrometer with a liquid nitrogen cooled MCT-A detector, a photoelastic modulator (HINDS Instruments PEM-90), and a demodulator (GWC Instruments) [36]. The p- and s-polarized infrared beam was generated with a ZnSe crystal driven with the photoelastic modulator at 50 kHz. The (p + s) and (p - s) signals of the reflected beam were recorded simultaneously with the demodulator. The reported spectrum in this paper is the (p-s)/(p+s) ratio under various humid conditions and all spectra were normalized with the spectrum obtained in dry nitrogen condition. Moreover, graphite and gold surfaces coated with the same amount of a Langmuir–Blodgett film of dimethyldioctadecylammonium bromide were also analyzed with PM-RAIRS to determine the relative sensitivity of PM-RAIRS for detection of adsorbates on these surfaces (see Supplementary Materials for details); this allowed to estimate the amount of water molecules adsorbed on the graphite surface.

2.2. Nanoscale friction measurement

The topographic scanning and friction measurements were performed at room temperature with AFM (SPI3800 N, Seiko, Japan) equipped with an environment control chamber. A Si_3N_4 tip (MLCT, Veeco, USA) with nominal radius less than 20 nm attached to an AFM cantilever was used in the friction and topography characterizations. The normal spring constant of the cantilever was calibrated as ~0.1 N/m by thermal noise method using an MFP-3DTM AFM (Asylum Research, CA, USA). Friction tests were carried out in two environmental conditions: (i) in vacuum condition with a pressure less than 10^{-4} Pa and (ii) in humid air condition with a relative humidity (RH) of $50 \pm 2\%$. The applied normal load ranged from 0 nN to 25 nN, and the tip sliding speed was 50 nm/s. The friction forces measured by the AFM tips were calibrated by using a silicon grating with a wedge angle of $54^{\circ}44'$ (TGF11, MikroMasch, Germany) [37].

3. Results and discussion

3.1. Chemical characterization of freshly-cleaved graphite surface

The freshly-cleaved graphite surface was analyzed with XPS without any sputter cleaning in vacuum. The survey spectrum in Fig. 1a shows a tiny signal of O 1s (532.7 eV), indicating the presence of a trace amount of oxygenated species at the surface. The C1s high-resolution spectrum (inset in Fig. 1a) can be fitted with one single peak centered at 284.5 eV with the Doniach—Sunjic line shape and the π - π * shake-up component at 291 eV [38]. No other component is necessary to improve the fit result. This implies that the freshly cleaved graphite surface contains intact graphene basal planes with very little defects (less than the detection limit of XPS). The small amount of oxygen detected in the survey spectrum should be due to oxygenated groups formed at the step edges via

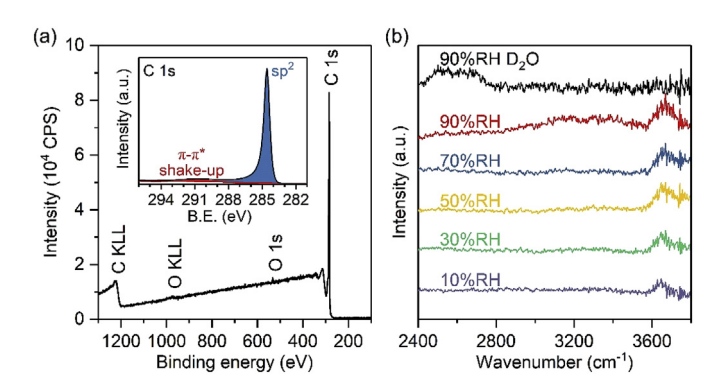


Fig. 1. Chemical characterization of newly-generated HOPG surfaces. (a) Survey XPS spectrum of the freshly-cleaved graphite surface exposed by tape-exfoliation of HOPG in ambient air. The inset is the C1s high-resolution XPS spectrum. (b) PM-RAIRS spectra of the freshly-cleaved graphite surface in various humid conditions. The spectra taken in humid conditions were normalized with the spectrum collected in dry condition for baseline correction. (A colour version of this figure can be viewed online.)

reactions of dangling bonds produced upon mechanical exfoliation with oxygen and water molecules impinging from the gas phase.

To determine the chemical nature of the oxygenated species on the freshly-cleaved graphite surface, PM-RAIRS analysis was carried out. Fig. 1b displays the PM-RAIRS spectra of the graphite surface collected in various RH conditions. There is no discernible peak in the 2850-2950 cm⁻¹ region, indicating the surface is free of any organic contaminants. The small peak at 3640-3650 cm⁻¹ matches well with the stretching vibration position of the free alkoxide (C-OH) group without hydrogen bonding interactions with surrounding molecules [39,40]. As RH increases, this peak grows only marginally. Since PM-RAIRS detects only the surface normal components of dipoles [41], the growth of the 3640-3650 cm⁻¹ peak with increasing RH could mean that more C-OH groups are pointing off the surface plane upon interactions with water molecules impinging from the gas phase or that some water molecules adsorbed with a single hydrogen bond. But, such water molecules do not readily stay at the surface until the humidity approaches near saturation condition (RH 90%) [12]. The hydrogen-bonded OH groups of physisorbed or condensed water exhibit broad peak spanning over the 2800–3600 cm⁻¹ region [42,43]; however, this peak is negligible at RH below 90%. When the graphite surface is exposed to RH 90% of D₂O, the free C-OH group is exchanged to the C-OD group whose stretch peak (~2720 cm⁻¹) is somewhat overlapping with the broad peak of physisorbed D₂O (2300–2700 cm⁻¹). This confirms that the graphene step edge is terminated with C-OH groups. By comparing the PM-RAIRS spectra of graphite surface and Au surface (Fig. S2) [44], the average amount of water molecules adsorbed on the freshly-cleaved graphite surface at 70% RH is estimated to be less than 0.1% of the water molecules adsorbed on the gold surface at the same RH. Such extremely low value implies that C-OH groups are only at the graphene step edges. Because these hydroxyl (alkoxide) groups are formed by reactions of the dangling bonds at the step edge with water molecules from the gas phase, it is likely that there would be a stoichiometrically equal amount of C-H groups at the step edge. If oxygen molecules are involved in passivation of the dangling bonds at the step edge, then the concentration of the C-H terminated sites would be even lower.

3.2. Nanoscale friction behaviors of single-layer thick graphene step edges

Fig. 2a and Fig. 2b show the topography and friction image of a $1.5 \,\mu m \times 1.5 \,\mu m$ area of the freshly cleaved graphite surface. Fig. 2c sketches all step edges identified with a height difference of about 0.34 nm. The step edge marked with the red solid line in Fig. 2c gives extremely high friction compared to the basal plan friction. The trace (stepping-upward) and retrace (stepping-downward) scans of this step show quite different lateral force profiles (AA' in Fig. 2d). The step edge marked with the blue dashed line in Fig. 2c gives a small change in the lateral force signal with the same sign in both trace and retrace scans (BB' in Fig. 2d). Other three step edges marked with green dotted lines exhibit lateral forces almost identical to the basal plane friction (CC' in Fig. 2d). The pull-off force of the AFM tip measured on the basal plane before and after the scanning is not changed (Fig. S3). Considering that the pull-off force is closely related to the tip radius and surface contamination [45], it is believed that little wear was caused due to the sliding.

Fig. 3a, Fig. 3b and 3c present the high-resolution topography images of the AA', BB', and CC' regions of Fig. 2c, respectively. The same tip was used and scanned in the same direction to collect these images. The height profile perpendicular to the step edge of each image is shown in Fig. 3d. It can be clearly seen that the height of these three steps is about 0.34 nm, which is in accordance with

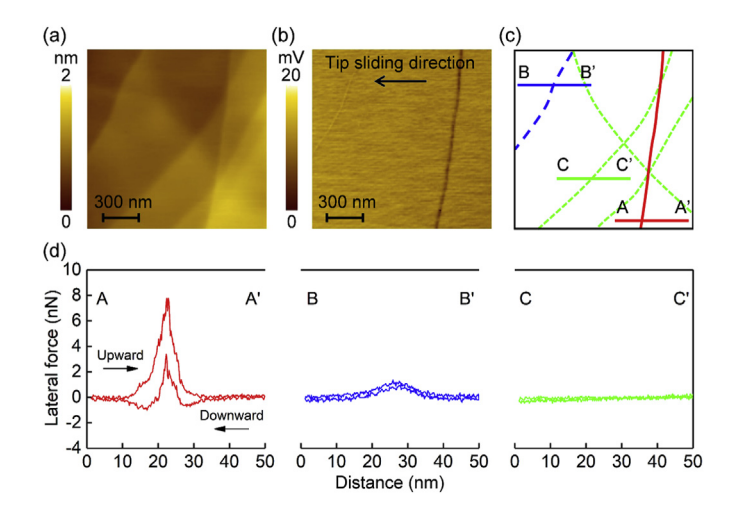


Fig. 2. Topography and friction on graphite surface measured by AFM with a Si_3N_4 tip. (a) Topography in a scan area of $1.5~\mu m \times 1.5~\mu m$. (b) Friction image measured in humid air under an applied load of 15~nN. (c) Schematic diagram showing all step edges. The red, blue, and green lines are the topographic steps identified with large, small, and negligible differences, respectively, from the basal plane friction. (d) Lateral forces measured along the lines marked as AA', BB', and CC'. (A colour version of this figure can be viewed online.)

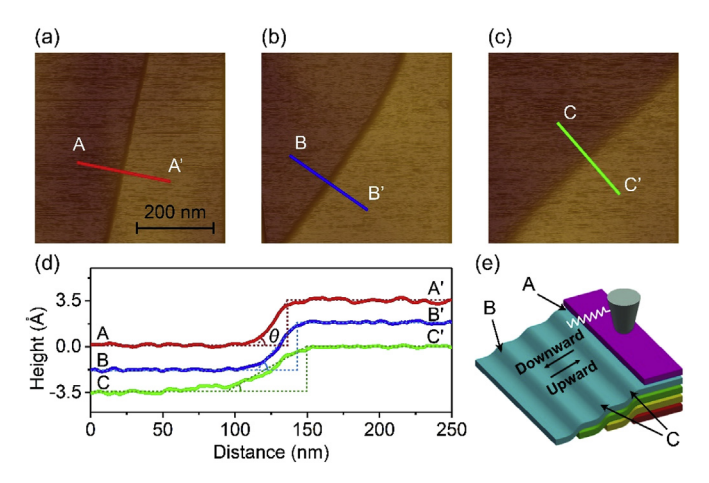


Fig. 3. (a, b, c) Topographies and (d) cross-section profiles at an exposed graphene step edge (AA'), a buried graphene step edge covered with one layer of graphene (BB'), and a buried graphene step edge covered with multi layers of graphene (CC'), respectively. (e) Illustration of such three different kinds of graphene step edges. (A colour version of this figure can be viewed online.)

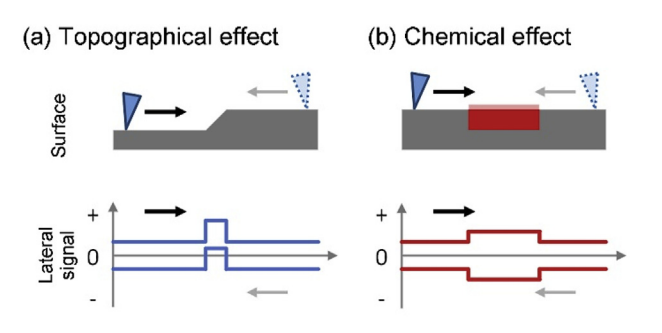
the thickness of a single layer graphene. However, the slope (θ) of the recorded topography is the smallest for the CC' edge (~30°), medium for the BB' edge (~50°), and the largest for the AA' edge (~60°). Probably, the largest angle is mostly governed by the curvature of the AFM tip in contact with the step edge [46]. Since the AA' step has the largest friction signal among all the step edges probed, we believe this is an exposed step edge without any other graphene layer covering it. This must be the place where the C—OH groups, which is detected with PM-RAIRS, are present along with C—H groups.

Because the friction signal of the BB' step edge is much weaker, but the step height is the same as the AA' step edge, the BB' step is believed to be a buried step edge, instead of being exposed to the gas phase. Considering the slight decrease in θ of the BB' step compared to the AA' step, it is believed that BB' step is covered probably with a single layer of graphene. The single graphene layer covering the step edge would be compliant due to the low bending

modulus, but still prevents the AFM tip from probing the deepest corner of the step edge [11]. Then, the CC' step with even smaller θ angle could be attributed to a step covered with multiple graphene layers. If multi-layer graphene is stiff enough, then the AFM tip will follow the topography of the topmost surface [37,47,48]. This is schematically illustrated in Fig. 3e.

Being able to distinguish the exposed and buried step edges with the same topographic height (around 0.34 nm) provides a good opportunity to investigate the effects of chemical functional groups present at the exposed step edge and topography change on lateral friction signal. The graphene edge buried under more than one layer of graphene (CC' in Fig. 3d) does not seem to add any additional resistance to the lateral sliding of the AFM tip (CC' in Fig. 2d). This might be because the slope or height derivative of the 0.34 nm thick topographic step covered with a stiff overlayer is not big enough to influence friction.

At the step edge buried under one layer of graphene (BB' in Fig. 3d), the lateral signal is shifted to the same direction during the step-up and step-down scans and the hysteresis between these two is almost the same as that observed on the basal plane (BB' in Fig. 2d). Such a behavior can be explained with the topographic artifact (geometry effect) in the lateral force measurement (Fig. 4a) [37,48]. The tip moving upward along the topographically-slanted surface experiences additional resistance than the tip moving on the flat surface (Fig. 5a, upper panel). For the same reason, the tip moving downward the slanted surface experiences less resistance (Fig. 5a, lower panel). Note that the sign of resistive and assistive force in Fig. 5a changes when the scan direction is reversed in AFM friction measurements. Such additional resistive (during step-up)



(c) Combination of topographical and chemical effects

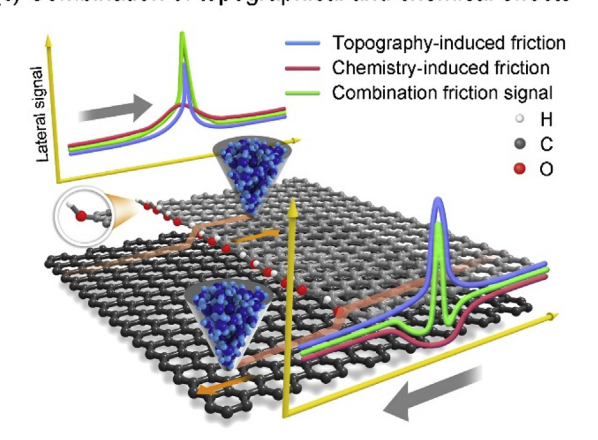


Fig. 4. Schematics of (a) topographic effect, (b) chemical effect and (c) the combination of topographic and chemical effects on the lateral signal when an AFM tip stepping upward and downward an exposed graphene step edge. Blue lines indicate topography-induced friction, red lines indicate chemistry-induced friction and green lines indicate the combined friction signal. (A colour version of this figure can be viewed online.)

and assistive (during step-down) forces due to topography change is a function of the slope angle, the COF, and the applied load [37,48]. Fig. 5b and c report the applied load dependence of the amount of shift in the lateral force signal (see Fig. S4 for the lateral force profiles). Both upward and downward scan directions show the same dependence on the applied load, and the environment (vacuum versus humid air) does not have any significant impact. The insensitivity of friction to the humidity change from 0% (vacuum) to ~50% (humid air) can be attributed to the lack of water adsorption on the graphite surface at RH below 90% (Fig. 1b).

In contrast to the friction response of the buried edge (BB' in Fig. 2d), the exposed edge (AA' in Fig. 2d) exhibits large hysteresis between the trace (step-up) and retrace (step-down). Such large differences in the lateral friction signal are quite remarkable when considering both AA' and BB' steps have the same height difference (0.34 nm) and similar slope angle. As shown in Fig. 6a, the lateral force signals of the AA' step edge could be fitted with two components — a narrow and large component (peak 1) and a broad and weak component (peak 2). It is noted that the peak 1 component is in the same direction in sign, i.e. resistive during the step-up and assistive during the step-down (similar to Fig. 5a). In contrast, the peak 2 component changes the sign when the scan direction is reversed, meaning it is resistive in both step-up and step-down scans.

Based on the similarity of the peak 1 component to the trend seen in Fig. 5a, it could be attributed to the topography-dominant effect. For the peak 2 component, the opposite sign in the lateral signal upon reversal of the scan direction (*i.e.*, resistive force in both trace and retrace directions) can be explained by the chemistry effect. If the substrate chemistry changes such that the adhesion or attractive interactions between the tip and surface increases, then the friction at that location will increase (Fig. 4b) [49,50]. Because there are C—OH groups at the step edge exposed to the gas phase (Fig. 1b), the Si₃N₄ tip surface will have stronger adhesive interactions with the substrate surface when it slides over the exposed step edge. Therefore, as shown in Fig. 4c, the lateral force of the AFM tip sliding across an exposed graphene step edge is affected by both topographic and chemical effects.

Fig. 6b plots the magnitude of the peak 1 component deconvoluted from the lateral signals measured for the exposed step edge at different applied loads in vacuum and humid air. Similar to the buried step edge case (Fig. 5b and c), the peak 1 component shows a linear dependence on the applied load and negligible dependence on the environment. This similarity supports that the peak 1 component must be dominantly due to the topographic effect. However, it is noted that its magnitude (Fig. 6b) is about one order of magnitude larger than the friction at buried step edge (Fig. 5b and c), although their topographic heights are the same and the slope angles are similar. The fact that it is exposed and chemicallyderivatized with highly polar groups appears to amplify the topographic effect in the lateral friction signal. One possible amplification mechanism might be the out-of-plane deformation of the C-OH groups at the step edge due to hydrogen bonding interactions with the tip surface during the step-up motion of the tip from the lower terrace to the upper terrace [51].

Fig. 6c plots the magnitude of the peak 2 component versus the applied load measured in vacuum and humid air environments. The load dependence of the step-up and step-down signals appears to be almost identical except the sign is opposite (so, both are resistive). Unlike the topography-dominant component (peak 1), the chemistry-dominant component (peak 2) shows small but noticeable dependence on the test environment. The resistive force due to the C–OH group at the exposed surface is slightly larger in humid air than that in vacuum. This could be associated with the slight increase in the free OH signal in the 3640-3650 cm⁻¹ region in the

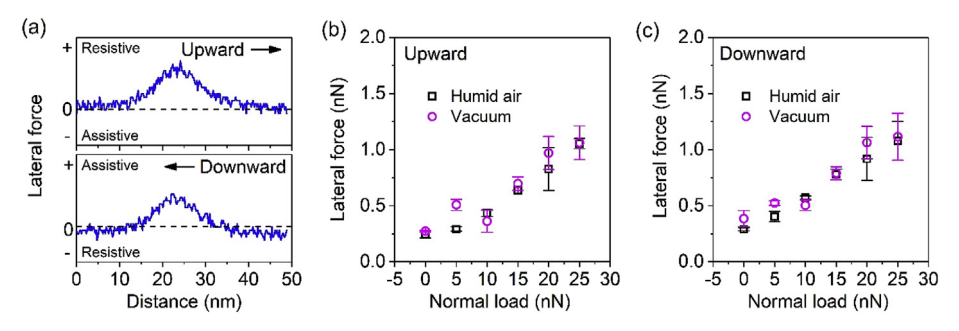


Fig. 5. Friction at the step edge covered with one layer of graphene measured in vacuum and humid air. (a) Typical lateral force curve at the step edge buried under a monolayer of graphene. (b, c) Maximum shift in the lateral force signal during the upward and downward sliding processes in vacuum and humid air conditions. (A colour version of this figure can be viewed online.)

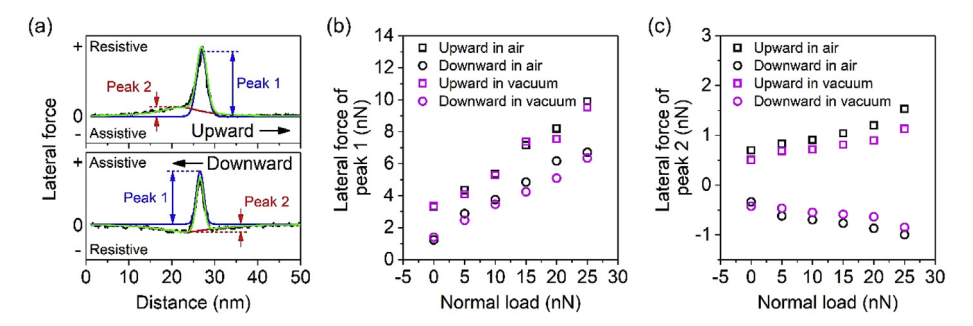


Fig. 6. Friction at the exposed step edge in vacuum and humid air. (a) Typical lateral force profiles of the upward and downward scans. The lateral force signals are fitted with two components (peak 1: blue line and peak 2: red line). (b, c) Applied load dependence of peak 1 and peak 2 components measured in vacuum and humid air. All raw data and fit results are shown in Fig. S4 and Fig. S5. (A colour version of this figure can be viewed online.)

PM-RAIRS as RH increases to 50% (Fig. 1b). It could also be due to the adsorption of water molecules at the native oxide surface of the AFM tip surface. In any case, the small difference in friction between the vacuum and ambient air conditions supports that the peak 2 component originates from hydrogen bonding interactions of the C—OH groups at the exposed step edge with the countersurface [51].

One could define the COF as $\mu = \Delta F_f / \Delta F_N$, where F_f is the measured friction force and F_N is the applied normal force. In other words, the slope of the least-square fit of the data shown in Fig. 5 for the buried step edge and Fig. 6 for the exposed step edge can be considered as the COF. Fig. 7 compares the COF values calculated from the linear fit of the data. The COF of the step edge covered with more than two layers of graphene is too small to be

determined (CC' in Fig. 2c). The step edge buried under one layer of graphene gives a COF of ~0.04. These results imply that the friction purely due to the 0.34 nm thick topographic corrugation is quite small. In contrast, the topographic effect of the exposed step edge of the same thickness is more than 5–6 times larger than that of the buried step edge. The chemistry effect due to the OH groups at the step edge gives a COF of 0.02–0.03 only (even smaller than the purely topographic effect of the 0.34 nm corrugation). The strong chemical interactions between the substrate surface and the sliding tip appear to significantly amplify the topographic effect.

Another set of friction test of buried and exposed graphene step edges was carried out with a different Si_3N_4 tip (Fig. S6). Although the magnitude of the lateral force is not exactly the same as the data presented in Figs. 5 and 6 due to the difference in tip radius, the

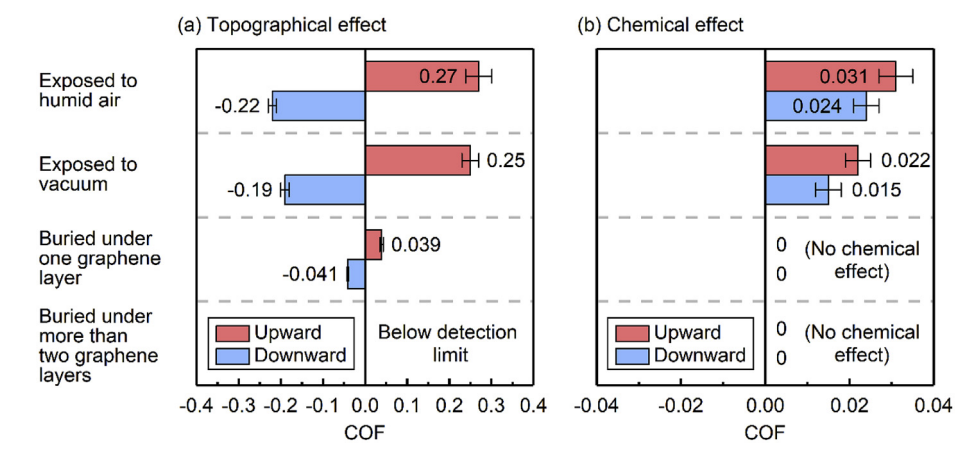


Fig. 7. COFs of (a) topographic effect and (b) chemical effect on various kinds of graphene step edges. The positive values imply the resistive force increases as the normal load grows, and the negative values imply the assistive force increases as the normal load grows. (A colour version of this figure can be viewed online.)

trends observed in the two sets of data are in good agreement to each other, confirming the reproducibility of the observed behavior.

In Fig. 6a, it is noted that the maximum position of the peak 2 component exists always in the lower terrace side of the maximum position of the peak 1 component (more data in Fig. S4 and Fig. S5). Considering the sp² hybridization of the carbon atoms to which the OH groups are attached, it is expected that the C-OH groups at the exposed edge point toward the lower terrace of the step (Fig. 4c). Thus, the chemical (hydrogen bonding) interactions between the tip and the C-OH groups would be the largest when the tip approaches the edge from the lower terrace in the step-up scan and departs from the edge onto the lower terrace in the step-down scan. This supports the hypothesis that the barrier resisting the tip sliding motion from the upper terrace of the exposed step edge of graphene to the lower terrace must be due to the C–OH groups formed when the new step edge is exposed to air during the mechanical exfoliation (Fig. 1b). This might be the origin of the Ehrlich-Schwoebel barrier in the case of graphene step edges. Note that, unlike the conventional concept of the Ehrlich-Schwoebel barrier which conjectures that the barrier exists at the upper terrace side of the step edge [34], the maximum resistance exists at the lower terrace side of the step edge.

When the lateral resolution scan is high enough (as in our experiment, 512 points of data were collected along the distance of 50 nm), then the topography-dominant (peak 1) and chemistry-dominant (peak 2) effects can be resolved easily [52]. When the lateral resolution scan is not high enough, one may see only resistive effect (when peak 2 > peak 1) [17–27] or assistive effect (when peak 1 > peak 2) [28,29]. Whether the topography effect or the chemical effect is dominant will depend on the system – surface chemistry of the tip as well as the applied normal load.

4. Conclusion

This study elucidated the friction behaviors of the 0.34 nm thick step edge of a single layer graphene. The graphene step edge exposed to air is terminated with the C-OH groups and probably equal amounts of C-H groups. Water molecules impinging from humid air does not physisorb readily to the step edge OH groups until the RH approaches the saturation point. The friction at this step edge can be deconvoluted to two components - one is the physical response due to the topographic height change and the other is the chemical response due to the presence of OH groups at the step edge. The step buried under graphene layers has very small topographic effect only. The exposed step edge of the same height has chemical effect due to the presence of OH groups, which substantially amplify the topographic effect. The synergistic effects of these chemical and topographic effects lead to a large COF. The maximum of the resistive force due to chemical effects, which can be attributed to the Ehrlich-Schwoebel barrier, is located at the lower terrace side of the step edge, not at the end of the upper

Author contributions

S.H.K. and L.Q. conceived the concept, L.Q., Z.Z. and L.C. designed and supervised AFM experiments, X.T. and W.Y. conducted AFM measurements, Z.C. carried out chemical analysis. S.H.K., L.Q., L.C., and Z.C. analyzed the data and wrote the manuscript. All authors have given approval to the final version of the manuscript.

Acknowledgements

This work was supported by the National Science Foundation (Grant No. CMMI-1727571) and the National Natural Science

Foundation of China (51875486 and 51527901). The HOPG sample used in this study was generously provided by Dr. Sudarshan Natarajan at Momentive Performance Materials.

Appendix A. Supplementary data

Supplementary data to this article can be found online at https://doi.org/10.1016/j.carbon.2019.07.081.

References

- [1] D. Berman, A. Erdemir, A.V. Sumant, Graphene: a new emerging lubricant, Mater. Today 17 (1) (2014) 31–42.
- [2] O. Penkov, H.-J. Kim, H.-J. Kim, D.-E. Kim, Tribology of graphene: a review, Int. J. Precis. Eng. Manuf. 15 (3) (2014) 577–585.
- [3] K.-S. Kim, H.-J. Lee, C. Lee, S.-K. Lee, H. Jang, J.-H. Ahn, et al., Chemical vapor deposition-grown graphene: the thinnest solid lubricant, ACS Nano 5 (6) (2011) 5107–5114
- [4] D. Berman, A. Erdemir, A.V. Sumant, Reduced wear and friction enabled by graphene layers on sliding steel surfaces in dry nitrogen, Carbon 59 (2013) 167–175.
- [5] D. Berman, A. Erdemir, A.V. Sumant, Graphene as a protective coating and superior lubricant for electrical contacts, Appl. Phys. Lett. 105 (23) (2014) 231907.
- [6] P. Wu, X. Li, C. Zhang, X. Chen, S. Lin, H. Sun, et al., Self-assembled graphene film as low friction solid lubricant in macroscale contact, ACS Appl. Mater. Interfaces 9 (25) (2017) 21554—21562.
- [7] D. Berman, S.A. Deshmukh, S.K.R.S. Sankaranarayanan, A. Erdemir, A.V. Sumant, Macroscale superlubricity enabled by graphene nanoscroll formation, Science 348 (6239) (2015) 1118–1122.
- [8] S.-W. Liu, H.-P. Wang, Q. Xu, T.-B. Ma, G. Yu, C. Zhang, et al., Robust microscale superlubricity under high contact pressure enabled by graphene-coated microsphere, Nat. Commun. 8 (2017) 14029.
- [9] Y. Song, D. Mandelli, O. Hod, M. Urbakh, M. Ma, Q. Zheng, Robust microscale superlubricity in graphite/hexagonal boron nitride layered heterojunctions, Nat. Mater. 17 (10) (2018) 894–899.
- [10] C. Lee, Q. Li, W. Kalb, X.-Z. Liu, H. Berger, R.W. Carpick, et al., Frictional characteristics of atomically thin sheets, Science 328 (5974) (2010) 76–80.
- [11] M.B. Elinski, Z. Liu, J.C. Spear, J.D. Batteas, 2D or not 2D? The impact of nanoscale roughness and substrate interactions on the tribological properties of graphene and MoS₂, J. Phys. D Appl. Phys. 50 (10) (2017) 103003.
- [12] H. Lee, J.-H. Ko, J.S. Choi, J.H. Hwang, Y.-H. Kim, M. Salmeron, et al., Enhancement of friction by water intercalated between graphene and mica, J. Phys. Chem. Lett. 8 (15) (2017) 3482—3487.
- [13] H. Lee, J.-H. Ko, H.C. Song, M. Salmeron, Y.-H. Kim, J.Y. Park, Isotope- and thickness-dependent friction of water layers intercalated between graphene and mica, Tribol. Lett. 66 (1) (2018) 36.
- [14] B.-C. Tran-Khac, H.-J. Kim, F.W. DelRio, K.-H. Chung, Operational and environmental conditions regulate the frictional behavior of two-dimensional materials, Appl. Surf. Sci. 483 (2019) 34–44.
- [15] Q. Li, X.-Z. Liu, S.-P. Kim, V.B. Shenoy, P.E. Sheehan, J.T. Robinson, et al., Fluorination of graphene enhances friction due to increased corrugation, Nano Lett. 14 (9) (2014) 5212–5217.
- [16] D. Berman, A. Erdemir, A.V. Zinovev, A.V. Sumant, Nanoscale friction properties of graphene and graphene oxide, Diam. Relat. Mater. 54 (2015) 91–96.
- [17] Y. Qi, J. Liu, Y. Dong, X.-Q. Feng, Q. Li, Impacts of environments on nanoscale wear behavior of graphene: edge passivation vs. substrate pinning, Carbon 139 (2018) 59–66.
- [18] H. Lang, Y. Peng, X. Zeng, X.a. Cao, L. Liu, K. Zou, Effect of relative humidity on the frictional properties of graphene at atomic-scale steps, Carbon 137 (2018) 519–526.
- [19] H. Lang, Y. Peng, X. Zeng, Effect of interlayer bonding strength and bending stiffness on 2-dimensional materials' frictional properties at atomic-scale steps, Appl. Surf. Sci. 411 (2017) 261–270.
- [20] B. Vasić, A. Matković, R. Gajić, I. Stanković, Wear properties of graphene edges probed by atomic force microscopy based lateral manipulation, Carbon 107 (2016) 723-732.
- [21] Z. Ye, A. Otero-de-la-Roza, E.R. Johnson, A. Martini, Effect of tip shape on atomic-friction at graphite step edges, Appl. Phys. Lett. 103 (8) (2013), 081601.
- [22] D.P. Hunley, T.J. Flynn, T. Dodson, A. Sundararajan, M.J. Boland, D.R. Strachan, Friction, adhesion, and elasticity of graphene edges, Phys. Rev. B 87 (3) (2013), 035417.
- [23] S. Panigrahi, A. Bhattacharya, D. Bandyopadhyay, S.J. Grabowski, D. Bhattacharyya, S. Banerjee, Wetting property of the edges of monoatomic step on graphite: frictional-force microscopy and ab initio quantum chemical studies, J. Phys. Chem. C 115 (30) (2011) 14819—14826.
- [24] H. Hölscher, D. Ebeling, U.D. Schwarz, Friction at atomic-scale surface steps: experiment and theory, Phys. Rev. Lett. 101 (24) (2008) 246105.
- [25] T. Müller, M. Lohrmann, T. Kässer, O. Marti, J. Mlynek, G. Krausch, Frictional force between a sharp asperity and a surface step, Phys. Rev. Lett. 79 (25)

- (1997) 5066-5069.
- [26] E. Weilandt, A. Menck, O. Marti, Friction studies at steps with friction force microscopy, Surf. Interface Anal. 23 (6) (1995) 428–430.
- [27] J.A. Ruan, B. Bhushan, Frictional behavior of highly oriented pyrolytic graphite, J. Appl. Phys. 76 (12) (1994) 8117—8120.
- [28] Z. Ye, A. Martini, Atomic friction at exposed and buried graphite step edges: experiments and simulations, Appl. Phys. Lett. 106 (23) (2015) 231603.
- [29] P. Egberts, Z. Ye, X.Z. Liu, Y. Dong, A. Martini, R.W. Carpick, Environmental dependence of atomic-scale friction at graphite surface steps, Phys. Rev. B 88 (3) (2013), 035409.
- [30] H. Lee, H.-B.-R. Lee, S. Kwon, M. Salmeron, J.Y. Park, Internal and external atomic steps in graphite exhibit dramatically different physical and chemical properties, ACS Nano 9 (4) (2015) 3814–3819.
- [31] R. Overney, E. Meyer, Tribological investigations using friction force microscopy, MRS Bull. 18 (5) (1993) 26–34.
- [32] S. Grafström, J. Ackermann, T. Hagen, R. Neumann, O. Probst, Analysis of lateral force effects on the topography in scanning force microscopy, J. Vac. Sci. Technol. B: Microelectron. Nanomater Struct. Process. Meas. 12 (3) (1994) 1559–1564.
- [33] S. Sundararajan, B. Bhushan, Topography-induced contributions to friction forces measured using an atomic force/friction force microscope, J. Appl. Phys. 88 (8) (2000) 4825–4831.
- [34] R.L. Schwoebel, E.J. Shipsey, Step motion on crystal surfaces, J. Appl. Phys. 37 (10) (1966) 3682–3686.
- [35] Y. Dong, X.Z. Liu, P. Egberts, Z. Ye, R.W. Carpick, A. Martini, Correlation between probe shape and atomic friction peaks at graphite step edges, Tribol. Lett. 50 (1) (2013) 49–57.
- [36] B.J. Barner, M.J. Green, E.I. Saez, R.M. Corn, Polarization modulation fourier transform infrared reflectance measurements of thin films and monolayers at metal surfaces utilizing real-time sampling electronics, Anal. Chem. 63 (1) (1991) 55–60
- [37] M. Varenberg, I. Etsion, G. Halperin, An improved wedge calibration method for lateral force in atomic force microscopy, Rev. Sci. Instrum. 74 (7) (2003) 3362–3367.
- [38] H. Estrade-Szwarckopf, XPS photoemission in carbonaceous materials: a "defect" peak beside the graphitic asymmetric peak, Carbon 42 (8) (2004) 1713—1721.
- [39] N. Chakroune, G. Viau, S. Ammar, N. Jouini, P. Gredin, M.J. Vaulay, et al.,

- Synthesis, characterization and magnetic properties of disk-shaped particles of a cobalt alkoxide: $Co^{II}(C_2H_4O_2)$, New J. Chem. 29 (2) (2005) 355–361.
- [40] G. Levita, P. Restuccia, M.C. Righi, Graphene and MoS₂ interacting with water: a comparison by *ab initio* calculations, Carbon 107 (2016) 878–884.
- [41] W.G. Golden, D.D. Saperstein, M.W. Severson, J. Overend, Infrared reflectionabsorption spectroscopy of surface species: a comparison of fourier transform and dispersion methods, J. Phys. Chem. 88 (3) (1984) 574–580.
- [42] A. Tu, H.R. Kwag, A.L. Barnette, S.H. Kim, Water adsorption isotherms on CH₃-, OH-, and COOH-terminated organic surfaces at ambient conditions measured with pm-rairs, Langmuir 28 (43) (2012) 15263–15269.
- [43] D.B. Asay, S.H. Kim, Evolution of the adsorbed water layer structure on silicon oxide at room temperature, J. Phys. Chem. B 109 (35) (2005) 16760–16763.
- [44] T. Buffeteau, B. Desbat, J.M. Turlet, Polarization modulation FT-IR spectroscopy of surfaces and ultra-thin films: experimental procedure and quantitative analysis, Appl. Spectrosc. 45 (3) (1991) 380–389.
- [45] B.V. Derjaguin, V.M. Muller, Y.P. Toporov, Effect of contact deformations on the adhesion of particles, J. Colloid Interface Sci. 53 (2) (1975) 314–326.
- [46] Z. Chen, J. Luo, I. Doudevski, S. Erten, S.H. Kim, Atomic force microscopy (AFM) analysis of an object larger and sharper than the AFM tip, Microsc. Microanal. (2019), https://doi.org/10.1017/S1431927619014697.
- [47] J.C. Spear, J.P. Custer, J.D. Batteas, The influence of nanoscale roughness and substrate chemistry on the frictional properties of single and few layer graphene, Nanoscale 7 (22) (2015) 10021–10029.
- [48] D.F. Ogletree, R.W. Carpick, M. Salmeron, Calibration of frictional forces in atomic force microscopy, Rev. Sci. Instrum. 67 (9) (1996) 3298–3306.
- [49] J.R. Felts, A.J. Oyer, S.C. Hernández, K.E. Whitener Jr., J.T. Robinson, S.G. Walton, et al., Direct mechanochemical cleavage of functional groups from graphene, Nat. Commun. 6 (2015) 6467.
- [50] A. Noy, C.D. Frisbie, L.F. Rozsnyai, M.S. Wrighton, C.M. Lieber, Chemical force microscopy: exploiting chemically-modified tips to quantify adhesion, friction, and functional group distributions in molecular assemblies, J. Am. Chem. Soc. 117 (30) (1995) 7943—7951.
- [51] Z. Chen, A. Khajeh, A. Martini, S.H. Kim, Chemical and physical origins of friction on surfaces with atomic steps, Sci. Adv. (2019), https://doi.org/ 10.1126/sciadv.aaw0513.
- [52] Z. Chen, S.H. Kim, Measuring nanoscale friction at graphene step edges, Friction, 2019 ([Under review]).